

WEIGHT-ADJUSTED DISCONTINUOUS GALERKIN METHODS: MATRIX-VALUED WEIGHTS WITH APPLICATION TO ELASTIC WAVE PROPAGATION

JESSE CHAN

Abstract. Weight-adjusted inner products [1, 2] replace weighted L^2 inner products with easily invertible weight-adjusted approximations. When paired with discontinuous Galerkin (DG) methods, the result is a low storage, energy stable, and (for sufficiently regular weights) high order accurate method for wave propagation in the presence of general heterogeneous media and curvilinear meshes. In this work, we extend weight-adjusted DG (WADG) methods to weighted inner products with matrix-valued weights, focusing on the linear elastic wave equation as an application. We present a new DG formulation based on the discretization of the symmetric form of the linear elasticity wave equation, with upwind-like dissipation incorporated through simple penalty terms in the numerical fluxes. This results in provably stable formulations for arbitrary anisotropic stiffness tensors and curvilinear meshes. A convergence analysis is given, and numerical results confirm the stability and high order accuracy of WADG for several problems in elastic wave propagation.

1. Introduction. There exist many high order energy stable discontinuous Galerkin formulations for the elastic wave equations in first order form. Wilcox et al. introduced a discontinuous Galerkin spectral element method on hexahedral meshes

SEM [3, 4]

High order DG [5, 6, 7, 8]

Interior penalty formulations. Analysis: Riviere et al. [9, 10] and Delcourte et al. [11, 12], dispersion analysis [13, 14].

GPU-accelerated DG methods [15, 16, 17]. Also elastic wave propagation and seismic wave applications [18, 19]

High order approximations of material data [20, 21], but not low storage or not energy stable.

Extending mass lumping without dispersive effects [22, 23]. Reduces to exact mass matrix inversion for constant weights.

A simpler extension of WADG [1, 2] to elasticity and weight-adjusted inner products for vector-valued functions.

Outline: present elasticity and an energy stable DG method, motivate need for alternative to inverting large dense coupled mass matrix, introduce weight-adjusted inner products.

2. Symmetric form of the elastic wave equation . We begin with the linear elastic wave equation under small deformations in a domain Ω . These equations can be written a first order velocity-stress system

$$\begin{aligned}\rho \frac{\partial \mathbf{v}}{\partial t} &= \nabla \cdot \mathbf{S} \\ \frac{\partial \mathbf{S}}{\partial t} &= \frac{1}{2} \bar{\mathbf{C}} (\nabla \mathbf{v} + \nabla \mathbf{v}^T),\end{aligned}$$

where \mathbf{v} is the velocity, \mathbf{S} is the stress tensor, ρ is density, and $\bar{\mathbf{C}}$ is the symmetric constitutive stiffness tensor relating stress and strain. These equations can also be rewritten as a symmetric hyperbolic system of PDEs [24]

$$\begin{aligned}\rho \frac{\partial \mathbf{v}}{\partial t} &= \sum_{i=1}^d \mathbf{A}_i^T \frac{\partial \boldsymbol{\sigma}}{\partial \mathbf{x}_i} \\ \mathbf{C}^{-1} \frac{\partial \boldsymbol{\sigma}}{\partial t} &= \sum_{i=1}^d \mathbf{A}_i \frac{\partial \mathbf{v}}{\partial \mathbf{x}_i}.\end{aligned}\tag{1}$$

where \mathbf{C} is the symmetric matrix form of the constitutive tensor $\bar{\mathbf{C}}$ and $\boldsymbol{\sigma}$ is a vector of length $N_d = \frac{d(d+1)}{2}$, the number of unique entries of the stress tensor \mathbf{S} . We note that the matrices \mathbf{A}_i are constant, while ρ and \mathbf{C} can vary spatially. Furthermore, we will assume that ρ and \mathbf{C} are positive-definite and bounded such that

$$\begin{aligned}\rho_{\min} &\leq \rho(\mathbf{x}) \leq \rho_{\max} \\ 0 &< c_{\min} \leq \mathbf{x}^T \mathbf{C} \mathbf{x} \leq c_{\max} < \infty, \quad \mathbf{x} \in \mathbb{R}^{N_d},\end{aligned}$$

which also implies that \mathbf{C}^{-1} is positive-definite and bounded.

In two dimensions, $\mathbf{v} = (\mathbf{v}_1, \mathbf{v}_2)^T$ and $\boldsymbol{\sigma} = (\sigma_{xx}, \sigma_{yy}, \sigma_{xy})^T$

$$\mathbf{S} = \begin{pmatrix} \sigma_{xx} & \sigma_{xy} \\ \sigma_{xy} & \sigma_{yy} \end{pmatrix}.$$

The matrices \mathbf{A}_i are given as

$$\mathbf{A}_1 = \begin{pmatrix} 1 & 0 \\ 0 & 0 \\ 0 & 1 \end{pmatrix}, \quad \mathbf{A}_2 = \begin{pmatrix} 0 & 0 \\ 0 & 1 \\ 1 & 0 \end{pmatrix}.$$

In three dimensions, the velocity is $\mathbf{v} = (\mathbf{v}_1, \mathbf{v}_2, \mathbf{v}_3)^T$, while $\boldsymbol{\sigma} = (\sigma_{xx}, \sigma_{yy}, \sigma_{zz}, \sigma_{yz}, \sigma_{xy}, \sigma_{xz})^T$ denotes the unique entries of the stress tensor \mathbf{S}

$$\mathbf{S} = \begin{pmatrix} \sigma_{xx} & \sigma_{xy} & \sigma_{xz} \\ \sigma_{xy} & \sigma_{yy} & \sigma_{yz} \\ \sigma_{xz} & \sigma_{yz} & \sigma_{zz} \end{pmatrix}.$$

The matrices \mathbf{A}_i are then

$$\mathbf{A}_1 = \begin{pmatrix} 1 & 0 & 0 \\ 0 & 0 & 0 \\ 0 & 0 & 0 \\ 0 & 0 & 0 \\ 0 & 0 & 1 \\ 0 & 1 & 0 \end{pmatrix}, \quad \mathbf{A}_2 = \begin{pmatrix} 0 & 0 & 0 \\ 0 & 1 & 0 \\ 0 & 0 & 0 \\ 0 & 0 & 1 \\ 0 & 0 & 0 \\ 1 & 0 & 0 \end{pmatrix}, \quad \mathbf{A}_3 = \begin{pmatrix} 0 & 0 & 0 \\ 0 & 0 & 0 \\ 0 & 0 & 1 \\ 0 & 1 & 0 \\ 1 & 0 & 0 \\ 0 & 0 & 0 \end{pmatrix}$$

In general anisotropic media, \mathbf{C} is symmetric and positive-definite. For two-dimensional isotropic media, \mathbf{C} is given as

$$\mathbf{C} = \begin{pmatrix} 2\mu + \lambda & \lambda & 0 \\ \lambda & 2\mu + \lambda & 0 \\ 0 & 0 & \mu \end{pmatrix},$$

where λ, μ are Lamé parameters. For three-dimensional isotropic media, \mathbf{C} is given instead by

$$\mathbf{C} = \begin{pmatrix} 2\mu + \lambda & \lambda & \lambda & & & \\ \lambda & 2\mu + \lambda & \lambda & & & \\ \lambda & \lambda & 2\mu + \lambda & & & \\ & & & \mu & & \\ & & & & \mu & \\ & & & & & \mu \end{pmatrix}.$$

We will consider both spatially varying isotropic and anisotropic media in this work.

3. An energy stable discontinuous Galerkin variational formulation. The advantage of the symmetric first order formulation of the elastic wave equations (1) is that it is straightforward to derive an energy stable discontinuous Galerkin formulation. We assume that the domain Ω is Lipschitz and exactly triangulated by a mesh Ω_h , which consists of elements D^k . We further assume that each element D^k is the image of a reference element \hat{D} under the local elemental mapping

$$\mathbf{x}^k = \boldsymbol{\Phi}^k \hat{\mathbf{x}},$$

where $\mathbf{x}^k = \{x^k, y^k, z^k\}$ denote physical coordinates on D^k and $\hat{\mathbf{x}} = \{\hat{x}, \hat{y}, \hat{z}\}$ denote coordinates on the reference element. We denote the determinant of the Jacobian of $\boldsymbol{\Phi}^k$ as J^k .

We will approximate components over each element D^k from an approximation space $V_h(D^k)$, which we defined as

$$V_h(D^k) = \boldsymbol{\Phi}^k \circ V_h(\hat{D}).$$

where $V_h(\widehat{D})$ is an approximation space defined on the reference element. For the remainder of this work, we will take $V_h(\widehat{D}) = P^N(\widehat{D})$, where $P^N(\widehat{D})$ is the polynomial space of total degree N on the reference simplex. In two dimensions,

$$P^N(\widehat{D}) = \{\widehat{x}^i \widehat{y}^j, \quad 0 \leq i + j \leq N\},$$

while in three dimensions,

$$P^N(\widehat{D}) = \{\widehat{x}^i \widehat{y}^j \widehat{z}^k, \quad 0 \leq i + j + k \leq N\}.$$

We denote the L^2 inner product and norm over D^k by $(\cdot, \cdot)_{L^2(D^k)}$, such that

$$(\mathbf{f}, \mathbf{g})_{L^2(D^k)} = \int_{D^k} \mathbf{f} \cdot \mathbf{g} \, dx = \int_{\widehat{D}} \mathbf{f} \cdot \mathbf{g} J^k, \quad \|\mathbf{f}\|_{L^2(D^k)}^2 = (\mathbf{f}, \mathbf{f})_{L^2(D^k)},$$

where \mathbf{f}, \mathbf{g} are vector-valued functions. Global L^2 inner products and norms are using local L^2 inner products and norms

$$(\mathbf{f}, \mathbf{g})_{\Omega_h} = \sum_{D^k \in \Omega_h} \int_{D^k} (\mathbf{f}, \mathbf{g})_{L^2(D^k)}, \quad \|\mathbf{f}\|_{\Omega_h}^2 = \sum_{D^k \in \Omega_h} \|\mathbf{f}\|_{L^2(D^k)}^2.$$

Let f be a face of an element D^k with neighboring element $D^{k,+}$ and unit outward normal \mathbf{n} . We define u^- and u^+ denote interior and exterior values of a discontinuous function u such that

$$u^- = u|_{f \cap D^k}, \quad u^+ = u|_{f \cap \partial D^{k,+}}.$$

The jump and average of a scalar function $u \in V_h(\Omega_h)$ over f are then defined as

$$[u] = u^+ - u^-, \quad \{u\} = \frac{u^+ + u^-}{2}.$$

Jumps and averages of a vector-valued functions $\mathbf{u} \in \mathbb{R}^m$ and $\mathbf{S} \in \mathbb{R}^{m \times n}$ are then defined component-wise

$$([\mathbf{u}])_i = [u_i], \quad 1 \leq i \leq m, \quad ([\mathbf{S}])_{ij} = [S_{ij}], \quad 1 \leq i \leq m, \quad 1 \leq j \leq n.$$

We can now specify a DG formulation for the linear elastic wave equation (1). Symmetric hyperbolic systems readily admit a DG formulation based on penalty fluxes, as detailed in [25]. For the linear elastic wave equation in symmetric first order form, this formulation is given as

$$(2) \quad \sum_{D^k \in \Omega_h} \left(\rho \frac{\partial \mathbf{v}}{\partial t}, \mathbf{w} \right)_{L^2(D^k)} = \sum_{D^k \in \Omega_h} \left(\left(\sum_{i=1}^d \mathbf{A}_i^T \frac{\partial \boldsymbol{\sigma}}{\partial \mathbf{x}_i}, \mathbf{w} \right)_{L^2(D^k)} + \left\langle \frac{1}{2} \mathbf{A}_n^T [\boldsymbol{\sigma}] + \frac{\tau_v}{2} \mathbf{A}_n^T \mathbf{A}_n [\mathbf{v}], \mathbf{w} \right\rangle_{L^2(\partial D^k)} \right)$$

$$\sum_{D^k \in \Omega_h} \left(\mathbf{C}^{-1} \frac{\partial \boldsymbol{\sigma}}{\partial t}, \mathbf{q} \right)_{L^2(D^k)} = \sum_{D^k \in \Omega_h} \left(\left(\sum_{i=1}^d \mathbf{A}_i \frac{\partial \mathbf{v}}{\partial \mathbf{x}_i}, \mathbf{q} \right)_{L^2(D^k)} + \left\langle \frac{1}{2} \mathbf{A}_n [\mathbf{v}] + \frac{\tau_\sigma}{2} \mathbf{A}_n \mathbf{A}_n^T [\boldsymbol{\sigma}], \mathbf{q} \right\rangle_{L^2(\partial D^k)} \right),$$

where $\tau_v, \tau_\sigma \geq 0$ are penalty parameters and \mathbf{A}_n is the normal matrix defined on a face f as $\mathbf{A}_n = \sum_{i=1}^d \mathbf{n}_i \mathbf{A}_i$. In two dimensions, \mathbf{A}_n is

$$\mathbf{A}_n = \begin{pmatrix} n_x & 0 \\ 0 & n_y \\ n_y & n_x \end{pmatrix}.$$

while in three dimensions, \mathbf{A}_n is

$$\mathbf{A}_n = \begin{pmatrix} n_x & 0 & 0 \\ 0 & n_y & 0 \\ 0 & 0 & n_z \\ 0 & n_z & n_y \\ n_z & 0 & n_x \\ n_y & n_z & 0 \end{pmatrix}.$$

3.1. Boundary conditions. In this work, we assume boundary conditions on velocity and traction of the form

$$\mathbf{v} = \mathbf{v}_{\text{bc}}, \quad \mathbf{S}\mathbf{n} = \mathbf{t}_{\text{bc}}$$

where \mathbf{v}_{bc} and \mathbf{t}_{bc} are given values. Traction boundary conditions where $\mathbf{t}_{\text{bc}} = 0$ are referred to as free-surface boundary conditions. We follow [26, 4] and impose boundary conditions on the DG formulation through exterior values and jumps of the solution. Boundary conditions on the normal component of the stress can be imposed by noting that the numerical flux contains the term $[\![\mathbf{A}_n^T \boldsymbol{\sigma}]\!] = \mathbf{S}\mathbf{n}$.

For a face which lies on a boundary, velocity boundary conditions are imposed by setting

$$[\![\mathbf{v}]\!] = 2(\mathbf{v}_{\text{bc}} - \mathbf{v}^-), \quad [\![\mathbf{A}_n^T \boldsymbol{\sigma}]\!] = [\![\mathbf{S}\mathbf{n}]\!] = 0,$$

while traction boundary conditions are imposed by

$$[\![\mathbf{A}_n^T \boldsymbol{\sigma}]\!] = [\![\mathbf{S}\mathbf{n}]\!] = 2(\mathbf{t}_{\text{bc}} - \mathbf{S}^-\mathbf{n}) = 2(\mathbf{t}_{\text{bc}} - \mathbf{A}_n^T \boldsymbol{\sigma}^-), \quad [\![\mathbf{v}]\!] = 0.$$

The numerical fluxes are then computed using these modified jumps.

For problems which involve the truncation of infinite or large domains, absorbing boundary conditions are required. For such cases, we impose simple non-reflective boundary conditions [26] through jumps

$$[\![\mathbf{A}_n^T \boldsymbol{\sigma}]\!] = [\![\mathbf{S}\mathbf{n}]\!] = -\mathbf{S}^-\mathbf{n} = -\mathbf{A}_n^T \boldsymbol{\sigma}^-, \quad [\![\mathbf{v}]\!] = -\mathbf{v}^-.$$

We note that more accurate absorbing conditions can be imposed using, for example, perfectly matched layers [27] or high order absorbing boundary conditions [28, 29].

3.2. Energy stability. It is straightforward to show that the formulation (3) is energy stable for zero velocity and traction boundary conditions, as well as non-reflective boundary conditions. Integrating by parts the velocity equations yields

$$(3) \quad \begin{aligned} \left(\rho \frac{\partial \mathbf{v}}{\partial t}, \mathbf{w} \right)_{L^2(D^k)} &= - \left(\sum_{i=1}^d \boldsymbol{\sigma}, \mathbf{A}_i \frac{\partial \mathbf{w}}{\partial \mathbf{x}_i} \right)_{L^2(D^k)} + \left\langle \mathbf{A}_n^T \{ \{ \boldsymbol{\sigma} \} \} + \frac{\tau_v}{2} \mathbf{A}_n^T \mathbf{A}_n [\![\mathbf{v}]\!], \mathbf{w} \right\rangle \\ \left(\mathbf{C}^{-1} \frac{\partial \boldsymbol{\sigma}}{\partial t}, \mathbf{q} \right)_{L^2(D^k)} &= \left(\sum_{i=1}^d \mathbf{A}_i \frac{\partial \mathbf{v}}{\partial \mathbf{x}_i}, \mathbf{q} \right)_{L^2(D^k)} + \left\langle \frac{1}{2} \mathbf{A}_n [\![\mathbf{v}]\!] + \frac{\tau_\sigma}{2} \mathbf{A}_n \mathbf{A}_n^T [\![\boldsymbol{\sigma}]\!], \mathbf{q} \right\rangle \end{aligned}$$

Taking $(\mathbf{w}, \mathbf{q}) = (\mathbf{v}, \boldsymbol{\sigma})$ and adding both equations together yields

$$\begin{aligned} \sum_{D^k \in \Omega_h} \frac{1}{2} \frac{\partial}{\partial t} \left((\rho \mathbf{v}, \mathbf{v})_{L^2(D^k)} + (\mathbf{C}^{-1} \boldsymbol{\sigma}, \boldsymbol{\sigma})_{L^2(D^k)} \right) &= \\ \sum_{D^k \in \Omega_h} \left\langle \mathbf{A}_n^T \{ \{ \boldsymbol{\sigma} \} \} + \frac{\tau_v}{2} \mathbf{A}_n^T \mathbf{A}_n [\![\mathbf{v}]\!], \mathbf{v} \right\rangle_{\partial D^k} &+ \left\langle \frac{1}{2} \mathbf{A}_n [\![\mathbf{v}]\!] + \frac{\tau_\sigma}{2} \mathbf{A}_n \mathbf{A}_n^T [\![\boldsymbol{\sigma}]\!], \boldsymbol{\sigma} \right\rangle_{\partial D^k} \\ \sum_{D^k \in \Omega_h} \sum_{f \in \partial D^k} \int_f \mathbf{A}_n^T \{ \{ \boldsymbol{\sigma} \} \} \mathbf{v} &+ \frac{\tau_v}{2} \mathbf{A}_n^T \mathbf{A}_n [\![\mathbf{v}]\!] \mathbf{v} + \frac{1}{2} \mathbf{A}_n [\![\mathbf{v}]\!] \boldsymbol{\sigma} + \frac{\tau_\sigma}{2} \mathbf{A}_n \mathbf{A}_n^T [\![\boldsymbol{\sigma}]\!] \boldsymbol{\sigma}. \end{aligned}$$

Let Γ_h denote the set of unique faces in Ω_h , and let $\Gamma_v, \Gamma_\sigma, \Gamma_{\text{abc}}$ denote the parts of the boundary where velocity, traction, and non-reflective boundary conditions are imposed, respectively. We separate surface terms into contributions from interior shared faces and from boundary faces. On interior shared faces,

$$\begin{aligned} \sum_{f \in \Gamma_h \setminus \partial \Omega} \int_f \mathbf{A}_n^T \{ \{ \boldsymbol{\sigma} \} \} \mathbf{v} &+ \frac{\tau_v}{2} \mathbf{A}_n^T \mathbf{A}_n [\![\mathbf{v}]\!] \mathbf{v} + \frac{1}{2} \mathbf{A}_n [\![\mathbf{v}]\!] \boldsymbol{\sigma} + \frac{\tau_\sigma}{2} \mathbf{A}_n \mathbf{A}_n^T [\![\boldsymbol{\sigma}]\!] \boldsymbol{\sigma} \\ \leq - \sum_{f \in \Gamma_h \setminus \partial \Omega} \int_f \frac{\tau_v}{2} |\mathbf{A}_n [\![\mathbf{v}]\!]|^2 &+ \frac{\tau_\sigma}{2} |\mathbf{A}_n^T [\![\boldsymbol{\sigma}]\!]|^2. \end{aligned}$$

For faces which lie on the boundary Γ_v where velocity boundary conditions are imposed, $[\![\mathbf{v}]\!] = -2\mathbf{v}^-$, $[\![\mathbf{A}_n^T \boldsymbol{\sigma}]\!] = 0$, and $\mathbf{A}_n^T \{\{\boldsymbol{\sigma}\}\} = \mathbf{S}\mathbf{n}^-$, implying that

$$\begin{aligned} & \sum_{f \in \Gamma_v} \int_f \mathbf{A}_n^T \{\{\boldsymbol{\sigma}\}\} \mathbf{v} + \frac{\tau_v}{2} \mathbf{A}_n^T \mathbf{A}_n [\![\mathbf{v}]\!] \mathbf{v} + \frac{1}{2} \mathbf{A}_n [\![\mathbf{v}]\!] \boldsymbol{\sigma} + \frac{\tau_\sigma}{2} \mathbf{A}_n \mathbf{A}_n^T [\![\boldsymbol{\sigma}]\!] \boldsymbol{\sigma} \\ &= \sum_{f \in \Gamma_v} \int_f \mathbf{A}_n^T \boldsymbol{\sigma}^- \mathbf{v}^- - \mathbf{A}_n \mathbf{v}^- \boldsymbol{\sigma}^- - \tau_v \mathbf{A}_n^T \mathbf{A}_n |\mathbf{v}^-|^2 = - \sum_{f \in \Gamma_v} \int_f \tau_v \mathbf{A}_n^T \mathbf{A}_n |\mathbf{v}^-|^2. \end{aligned}$$

For faces which lie on Γ_σ , $\mathbf{A}_n^T [\![\boldsymbol{\sigma}]\!] = -2\mathbf{A}_n^T \boldsymbol{\sigma}^-$, $\mathbf{A}_n^T \{\{\boldsymbol{\sigma}\}\} = 0$, and $[\![\mathbf{v}]\!] = 0$, yielding a similar contribution

$$\sum_{f \in \Gamma_\sigma} \int_f \mathbf{A}_n^T \{\{\boldsymbol{\sigma}\}\} \mathbf{v} + \frac{\tau_v}{2} \mathbf{A}_n^T \mathbf{A}_n [\![\mathbf{v}]\!] \mathbf{v} + \frac{1}{2} \mathbf{A}_n [\![\mathbf{v}]\!] \boldsymbol{\sigma} + \frac{\tau_\sigma}{2} \mathbf{A}_n \mathbf{A}_n^T [\![\boldsymbol{\sigma}]\!] \boldsymbol{\sigma} = - \sum_{f \in \Gamma_\sigma} \int_f \tau_\sigma \mathbf{A}_n \mathbf{A}_n^T |\boldsymbol{\sigma}^-|^2.$$

Finally, for faces in Γ_{abc} we have $\mathbf{A}_n^T \{\{\boldsymbol{\sigma}\}\} = \frac{1}{2} \mathbf{A}_n^T \boldsymbol{\sigma}^-$, $\mathbf{A}_n^T [\![\boldsymbol{\sigma}]\!] = -\mathbf{A}_n^T \boldsymbol{\sigma}^-$, and $[\![\mathbf{v}]\!] = -\mathbf{v}^-$, yielding

$$\begin{aligned} & \sum_{f \in \Gamma_{\text{abc}}} \int_f \mathbf{A}_n^T \{\{\boldsymbol{\sigma}\}\} \mathbf{v} + \frac{\tau_v}{2} \mathbf{A}_n^T \mathbf{A}_n [\![\mathbf{v}]\!] \mathbf{v} + \frac{1}{2} \mathbf{A}_n [\![\mathbf{v}]\!] \boldsymbol{\sigma} + \frac{\tau_\sigma}{2} \mathbf{A}_n \mathbf{A}_n^T [\![\boldsymbol{\sigma}]\!] \boldsymbol{\sigma} = \\ & - \sum_{f \in \Gamma_{\text{abc}}} \int_f \frac{\tau_v}{2} \mathbf{A}_n^T \mathbf{A}_n |\mathbf{v}^-|^2 + \frac{\tau_\sigma}{2} \mathbf{A}_n \mathbf{A}_n^T |\boldsymbol{\sigma}^-|^2. \end{aligned}$$

Combining these face contributions yields

$$\begin{aligned} & \sum_{D^k \in \Omega_h} \frac{1}{2} \frac{\partial}{\partial t} \left((\rho \mathbf{v}, \mathbf{v})_{L^2(D^k)} + (\mathbf{C}^{-1} \boldsymbol{\sigma}, \boldsymbol{\sigma})_{L^2(D^k)} \right) \leq - \sum_{f \in \Gamma_h \setminus \partial \Omega} \int_f \frac{\tau_v}{2} |\mathbf{A}_n [\![\mathbf{v}]\!]|^2 + \frac{\tau_\sigma}{2} |\mathbf{A}_n^T [\![\boldsymbol{\sigma}]\!]|^2 \\ (4) \quad & - \sum_{f \in \Gamma_v} \int_f \tau_v |\mathbf{A}_n \mathbf{v}^-|^2 - \sum_{f \in \Gamma_\sigma} \int_f \tau_\sigma |\mathbf{A}_n^T \boldsymbol{\sigma}^-|^2 - \sum_{f \in \Gamma_{\text{abc}}} \int_f \frac{\tau_v}{2} |\mathbf{A}_n \mathbf{v}^-|^2 + \frac{\tau_\sigma}{2} |\mathbf{A}_n^T \boldsymbol{\sigma}^-|^2 \leq 0. \end{aligned}$$

Since ρ and \mathbf{C}^{-1} are positive definite, the left hand side of (4) is an L^2 -equivalent norm on $(\mathbf{u}, \boldsymbol{\sigma})$

$$C_1 \|(\mathbf{u}, \boldsymbol{\sigma})\|_{L^2(\Omega)}^2 \leq \sum_{D^k \in \Omega_h} \frac{1}{2} \frac{\partial}{\partial t} \left((\rho \mathbf{v}, \mathbf{v})_{L^2(D^k)} + (\mathbf{C}^{-1} \boldsymbol{\sigma}, \boldsymbol{\sigma})_{L^2(D^k)} \right) \leq C_2 \|(\mathbf{u}, \boldsymbol{\sigma})\|_{L^2(\Omega)}^2$$

for $\|(\mathbf{u}, \boldsymbol{\sigma})\|_{L^2(\Omega)}^2 = \|\mathbf{u}\|_{L^2(\Omega)}^2 + \|\boldsymbol{\sigma}\|_{L^2(\Omega)}^2$. This implies that the DG formulation is energy stable and that the magnitude of the DG solution $(\mathbf{u}, \boldsymbol{\sigma})$ is non-increasing in time. This also shows that dissipation present for positive penalization constants τ_v, τ_σ acts on non-conforming components with non-zero jumps $\mathbf{A}_n^T [\![\mathbf{v}]\!]$ and $\mathbf{A}_n [\![\boldsymbol{\sigma}]\!]$. In fact, it was shown in [25] that, in the limit as $\tau_v, \tau_\sigma \rightarrow \infty$, the eigenspaces of DG discretizations split into a conforming part consisting of $\mathbf{u}, \boldsymbol{\sigma}$ which satisfy

$$\mathbf{A}_n [\![\mathbf{u}]\!] = 0, \quad \mathbf{A}_n^T [\![\boldsymbol{\sigma}]\!] = 0$$

and an non-conforming part (defined through the L^2 orthogonal complement) corresponding to eigenvalues contain real parts which approach $-\infty$. For the linear elastic wave equations, these conditions are equivalent to the requirement of C^0 continuity for \mathbf{u} and normal continuity of the stress tensor $[\![\mathbf{S}]\!] \mathbf{n} = 0$.

While this DG formulation is

4. Weight-adjusted approximation of vector-valued inner products. We also introduce the standard Lebesgue L^p norms over a general domain Ω

$$\begin{aligned} \|u\|_{L^p(\Omega)} &= \left(\int_\Omega u^p \right)^{1/p} \quad 1 \leq p < \infty \\ \|u\|_{L^\infty(\Omega)} &= \inf \{C \geq 0 : |u(\mathbf{x})| \leq C \quad \forall \mathbf{x} \in \Omega\}, \end{aligned}$$

and the associated L^p spaces

$$\begin{aligned} L^p(\Omega) &= \left\{ u : \Omega \rightarrow \mathbb{R}, \quad \|u\|_{L^p(\Omega)} < \infty \right\} \quad 1 \leq p < \infty \\ L^\infty(\Omega) &= \left\{ u : \Omega \rightarrow \mathbb{R}, \quad \|u\|_{L^\infty(\Omega)} < \infty \right\}. \end{aligned}$$

The L^p Sobolev seminorms and norms of degree s are then defined

$$\begin{aligned} |u|_{W^{s,p}(\Omega)} &= \left(\sum_{|\alpha|=s} \|D^\alpha u\|_{L^p(\Omega)}^p \right)^{1/p}, \quad |u|_{W^{s,\infty}(\Omega)} = \max_{|\alpha|=s} \|D^\alpha u\|_{L^\infty(\Omega)} \\ \|u\|_{W^{s,p}(\Omega)} &= \left(\sum_{|\alpha| \leq s} \|D^\alpha u\|_{L^p(\Omega)}^p \right)^{1/p}, \quad \|u\|_{W^{s,\infty}(\Omega)} = \max_{|\alpha| \leq s} \|D^\alpha u\|_{L^\infty(\Omega)}. \end{aligned}$$

where $\alpha = \{\alpha_1, \alpha_2, \alpha_3\}$ is a multi-index such that

$$D^\alpha u = \frac{\partial^{\alpha_1}}{\partial x^{\alpha_1}} \frac{\partial^{\alpha_2}}{\partial y^{\alpha_2}} \frac{\partial^{\alpha_3}}{\partial z^{\alpha_3}} u,$$

We define $D^\alpha \mathbf{v}$ as the component-wise derivative of \mathbf{v} with respect to a d -dimensional multi-index α

$$(D^\alpha \mathbf{v})_i = \frac{\partial^{\alpha_1}}{\partial x^{\alpha_1}} \frac{\partial^{\alpha_2}}{\partial x^{\alpha_2}} \frac{\partial^{\alpha_3}}{\partial x^{\alpha_3}} v_i.$$

We generalize the weight-adjusted scalar inner products introduced in [1, 2] to vector-valued inner products with matrix weights.

Vector Sobolev norms for $\mathbf{v}(\mathbf{x}) \in \mathbb{R}^m$ can be defined as

$$\begin{aligned} \|\mathbf{v}\|_{W^{k,p}}^p &= \sum_{i=1}^m \|\mathbf{v}_i\|_{W^{k,p}}^p = \sum_{|\alpha| \leq k} \|D^\alpha \mathbf{v}\|_{L^p}^p, \quad 1 \leq p < \infty, \\ \|\mathbf{v}\|_{W^{k,\infty}} &= \max_i \|\mathbf{v}_i\|_{W^{k,\infty}}. \end{aligned}$$

Let \mathbf{W} be a symmetric positive-definite matrix such that

$$0 < w_{\min} \leq \|\mathbf{W}(\mathbf{x})\|_2 \leq w_{\max} < \infty, \quad 0 < \tilde{w}_{\min} \leq \|\mathbf{W}^{-1}(\mathbf{x})\|_2 \leq \tilde{w}_{\max} < \infty, \quad \forall \mathbf{x} \in \Omega.$$

We define a k th order Sobolev norm for matrix-valued weight function $\mathbf{W}(\mathbf{x})$ in terms of the induced p -norm

$$\|\mathbf{W}(\mathbf{x})\|_{k,p}^p = \sum_{|\alpha| \leq k} \sup_{\mathbf{x}} \|D^\alpha \mathbf{W}(\mathbf{x})\|_p^p$$

While this norm is not sub-multiplicative, the following bound holds

$$\begin{aligned} \|\mathbf{W}\mathbf{v}\|_{W^{k,p}}^p &= \sum_{|\alpha| \leq k} \|D^\alpha (\mathbf{W}\mathbf{v})\|_{L^p}^p \leq C_N \int \sum_{|\alpha| \leq k} \sum_{|\beta| \leq |\alpha|} \|(D^\beta \mathbf{W})(D^{\alpha-\beta} \mathbf{v})\|_p^p \\ &\leq C_N \int \left(\sum_{|\alpha| \leq k} \|(D^\alpha \mathbf{W})\| \right)^p \left(\sum_{|\alpha| \leq k} \|D^\alpha \mathbf{v}\|_p \right)^p \\ &\leq C_N \|\mathbf{W}\|_{k,p}^p \|\mathbf{v}\|_{k,p}^p, \end{aligned}$$

where we have used Leibniz's rule, Cauchy-Schwarz, and the arithmetic-geometric mean inequality.

To show that weight-adjusted DG methods are high order accurate, we make use of a weighted interpolation estimate. The scalar version of this estimate is derived in [30, 1].

THEOREM 1 (Theorem 3.1 in [1]). Let D^k be a quasi-regular element with representative size $h = \text{diam}(D^k)$. For $N \geq 0$, $w \in W^{N+1,\infty}$, and $u \in W^{N+1,2}$,

$$\left\| u - \frac{1}{w} \Pi_N(wu) \right\|_{L^2(D^k)} \leq C_N h^{N+1} \left\| \sqrt{J} \right\|_{L^\infty(D^k)} \left\| \frac{1}{\sqrt{J}} \right\|_{L^\infty(D^k)} \left\| \frac{1}{w} \right\|_{L^\infty} \|w\|_{W^{N+1,\infty}} \|u\|_{W^{N+1,2}}.$$

For $w = 1$, this reduces to the standard interpolation estimate

$$\|u - \Pi_N u\|_{L^2(D^k)} \leq C h^{N+1} \|u\|_{W^{N+1,2}}.$$

Theorem 2 extends Theorem 1 to matrix weights by computing weighted interpolation estimates for the quantity $\mathbf{W}^{-1} \Pi_N(\mathbf{W} \mathbf{v})$.

THEOREM 2. Let D^k be a quasi-regular element with representative size $h = \text{diam}(D^k)$. For $N \geq 0$, $\mathbf{W} \in (W^{N+1,\infty})^{d \times d}$, and $\mathbf{v} \in (W^{N+1,2})^d$,

$$\|\mathbf{v} - \mathbf{W}^{-1} \Pi_N(\mathbf{W} \mathbf{v})\|_{L^2} \leq C h^{N+1} \left\| \sqrt{J} \right\|_{L^\infty(D^k)} \left\| \frac{1}{\sqrt{J}} \right\|_{L^\infty(D^k)} \tilde{w}_{\max} \|\mathbf{W}\|_{N+1} \|\mathbf{v}\|_{W^{N+1,2}}$$

Proof. The proof is the similar to the scalar case. Using vector-valued versions of Bramble-Hilbert and a scaling argument for quasi-regular elements yields

$$\begin{aligned} \|\mathbf{v} - \mathbf{W}^{-1} \Pi_N(\mathbf{W} \mathbf{v})\|_{L^2} &\leq C_1 \left\| \sqrt{J} \right\|_{L^\infty(D^k)} \sup_{\mathbf{x}} \|\mathbf{W}^{-1}\|_2 \|\mathbf{W} \mathbf{v} - \Pi_N(\mathbf{W} \mathbf{v})\|_{L^2} \\ &\leq C_1 \left\| \sqrt{J} \right\|_{L^\infty(D^k)} \sup_{\mathbf{x}} \|\mathbf{W}^{-1}\|_2 |\mathbf{W} \mathbf{v}|_{W^{N+1,2}(\hat{D})} \\ &\leq C_2 h^{N+1} \left\| \sqrt{J} \right\|_{L^\infty(D^k)} \left\| \frac{1}{\sqrt{J}} \right\|_{L^\infty(D^k)} \sup_{\mathbf{x}} \|\mathbf{W}^{-1}\|_2 \|\mathbf{W} \mathbf{v}\|_{W^{N+1,2}(D^k)} \\ &\leq C_3 h^{N+1} \left\| \sqrt{J} \right\|_{L^\infty(D^k)} \left\| \frac{1}{\sqrt{J}} \right\|_{L^\infty(D^k)} \tilde{w}_{\max} \|\mathbf{W}\|_{W^{N+1,2}} \|\mathbf{v}\|_{W^{N+1,2}(D^k)}. \quad \square \end{aligned}$$

4.1. Properties of weight-adjusted vector-valued inner products. Let Π_N be the L^2 projection applied to each component of a vector. Define the operator $T_{\mathbf{W}}$

$$T_{\mathbf{W}} \mathbf{v} = \Pi_N(\mathbf{W} \mathbf{v})$$

The inverse operator $T_{\mathbf{W}}^{-1}$ is defined implicitly via

$$(\mathbf{W} T_{\mathbf{W}}^{-1} \mathbf{v}, \mathbf{w}) = (\mathbf{v}, \mathbf{w}).$$

These definitions generalize $T_{\mathbf{W}}$ to matrix-valued \mathbf{W} . Conveniently, all properties of $T_{\mathbf{W}}$ for scalar \mathbf{W} carry over from [1].

LEMMA 3. Let Π_N denote the component-wise L^2 projection, and let $\mathbf{W} \in (L^\infty)^m$. Then, $T_{\mathbf{W}}$ satisfies the following properties:

1. $T_{\mathbf{W}}^{-1} T_{\mathbf{W}} = \Pi_N$
2. $\Pi_N T_{\mathbf{W}}^{-1} = T_{\mathbf{W}}^{-1} \Pi_N = T_{\mathbf{W}}^{-1}$
3. $\|T_{\mathbf{W}}^{-1}\|_{L^2(D^k)} \leq \tilde{w}_{\max}$.
4. $(T_{\mathbf{W}}^{-1} \mathbf{v}, \mathbf{w})$ forms an inner product on $(P^N)^m \times (P^N)^m$, which is equivalent to the L^2 inner product with equivalence constants $C_1 = \tilde{w}_{\min}$, $C_2 = \tilde{w}_{\max}$.

Proof. The proofs of properties 1 and 2 are consequences of the definition of $T_{\mathbf{W}}$, and are identical to proofs for the scalar case. Property 3 is a straightforward extension from the scalar case. Let $\mathbf{v} \in (P^N)^m$. Then,

$$(T_{\mathbf{W}}^{-1} \mathbf{v}, \mathbf{v}) = (\mathbf{W}^{-1} \mathbf{W} T_{\mathbf{W}}^{-1} \mathbf{v}, \mathbf{v}) \leq \sup_{\mathbf{x}} \|\mathbf{W}^{-1}(\mathbf{x})\| (\mathbf{W} T_{\mathbf{W}}^{-1} \mathbf{v}, \mathbf{v}) = \tilde{w}_{\max} \|\mathbf{v}\|_{L^2}^2.$$

Property 4 then simply requires the lower bound

$$(T_{\mathbf{W}}^{-1} \mathbf{v}, \mathbf{v}) = (\mathbf{W}^{-1} \mathbf{W} T_{\mathbf{W}}^{-1} \mathbf{v}, \mathbf{v}) \geq \inf_{\mathbf{x}} \|\mathbf{W}^{-1}(\mathbf{x})\| \|\mathbf{v}\|_{L^2}^2 = \tilde{w}_{\min} \|\mathbf{v}\|_{L^2}^2. \quad \square$$

Using Theorem 2, we may also show that the matrix-valued weight-adjusted inner product is also high order accurate for sufficiently regular \mathbf{W} .

THEOREM 4. *Let D^k be a quasi-regular element with representative size $h = \text{diam}(D^k)$. For $N > 0$*

$$\|\mathbf{W} \mathbf{v} - T_{\mathbf{W}^{-1}}^{-1} \mathbf{v}\|_{L^2(D^k)} \leq C_{\mathbf{W}} h^{N+1} \|\mathbf{v}\|_{W^{N+1,2}(D^k)}$$

with constant $C_{\mathbf{W}}$ depending on \mathbf{W} and N

$$C_{\mathbf{W}} = C_N \left\| \sqrt{J} \right\|_{L^\infty(D^k)} \left\| \frac{1}{\sqrt{J}} \right\|_{L^\infty(D^k)} \tilde{w}_{\max} w_{\max} \|\mathbf{W}\|_{W^{N+1,2}(D^k)}.$$

Proof. The proof is again similar to the scalar case. The triangle inequality gives

$$\|\mathbf{W} \mathbf{v} - T_{\mathbf{W}^{-1}}^{-1} \mathbf{v}\|_{L^2(D^k)} \leq \|\mathbf{W} \mathbf{v} - \Pi_N(\mathbf{W} \mathbf{v})\|_{L^2(D^k)} + \|\Pi_N(\mathbf{W} \mathbf{v}) - T_{\mathbf{W}^{-1}}^{-1} \mathbf{v}\|_{L^2(D^k)}.$$

The former term is bounded by interpolation estimates and by arguments used in the proof of Theorem 2. The latter term is bounded

$$\begin{aligned} \|\Pi_N(\mathbf{W} \mathbf{v}) - T_{\mathbf{W}^{-1}}^{-1} \mathbf{v}\|_{L^2(D^k)} &= \|T_{\mathbf{W}^{-1}}^{-1} T_{\mathbf{W}^{-1}} \Pi_N(\mathbf{W} \mathbf{v}) - T_{\mathbf{W}^{-1}}^{-1} \Pi_N \mathbf{v}\|_{L^2(D^k)} \\ &= \|T_{\mathbf{W}^{-1}}^{-1} \Pi_N(T_{\mathbf{W}^{-1}} \Pi_N(\mathbf{W} \mathbf{v})) - T_{\mathbf{W}^{-1}}^{-1} \Pi_N \mathbf{v}\|_{L^2(D^k)} \\ &\leq C_N \|T_{\mathbf{W}^{-1}}^{-1}\| \|T_{\mathbf{W}^{-1}} \Pi_N(\mathbf{W} \mathbf{v}) - \Pi_N \mathbf{v}\|_{L^2(D^k)} \\ &\leq C_N \|T_{\mathbf{W}^{-1}}^{-1}\| \|\Pi_N(\mathbf{W}^{-1} \Pi_N(\mathbf{W} \mathbf{v})) - \Pi_N \mathbf{v}\|_{L^2(D^k)} \\ &\leq C_N w_{\max} \|\mathbf{W}^{-1} \Pi_N(\mathbf{W} \mathbf{v}) - \mathbf{v}\|_{L^2(D^k)}. \end{aligned}$$

where we have used $\|T_{\mathbf{W}^{-1}}^{-1}\| \leq w_{\max}$ (Lemma 3) and $\|\Pi_N\|_{L^2(D^k)} = 1$. An application of Theorem 2 to bound $\|\mathbf{W}^{-1} \Pi_N(\mathbf{W} \mathbf{v}) - \mathbf{v}\|_{L^2(D^k)}$ completes the proof. \square

5. A weight-adjusted discontinuous Galerkin method for elastic wave propagation. Recall the energy stable formulation for DG

$$\begin{aligned} \left(\rho \frac{\partial \mathbf{v}}{\partial t}, \mathbf{w} \right)_{L^2(D^k)} &= \left(\sum_{i=1}^d \mathbf{A}_i^T \frac{\partial \boldsymbol{\sigma}}{\partial \mathbf{x}_i}, \mathbf{w} \right)_{L^2(D^k)} + \left\langle \frac{1}{2} \mathbf{A}_n^T \llbracket \boldsymbol{\sigma} \rrbracket + \frac{\tau_v}{2} \mathbf{A}_n \mathbf{A}_n^T \llbracket \mathbf{v} \rrbracket, \mathbf{w} \right\rangle \\ \left(\mathbf{C}^{-1} \frac{\partial \boldsymbol{\sigma}}{\partial t}, \mathbf{q} \right)_{L^2(D^k)} &= \left(\sum_{i=1}^d \mathbf{A}_i \frac{\partial \mathbf{v}}{\partial \mathbf{x}_i}, \mathbf{q} \right)_{L^2(D^k)} + \left\langle \frac{1}{2} \mathbf{A}_n \llbracket \mathbf{v} \rrbracket + \frac{\tau_\sigma}{2} \mathbf{A}_n^T \mathbf{A}_n \llbracket \boldsymbol{\sigma} \rrbracket, \mathbf{q} \right\rangle. \end{aligned}$$

The weight-adjusted DG method simply replaces the weighted L^2 inner products appearing in the left hand side of this formulation with weight-adjusted approximations

$$\begin{aligned} \left(T_{1/\rho}^{-1} \frac{\partial \mathbf{v}}{\partial t}, \mathbf{w} \right)_{L^2(D^k)} &= \left(\sum_{i=1}^d \mathbf{A}_i^T \frac{\partial \boldsymbol{\sigma}}{\partial \mathbf{x}_i}, \mathbf{w} \right)_{L^2(D^k)} + \left\langle \frac{1}{2} \mathbf{A}_n^T \llbracket \boldsymbol{\sigma} \rrbracket + \frac{\tau_v}{2} \mathbf{A}_n \mathbf{A}_n^T \llbracket \mathbf{v} \rrbracket, \mathbf{w} \right\rangle \\ \left(T_{\mathbf{C}}^{-1} \frac{\partial \boldsymbol{\sigma}}{\partial t}, \mathbf{q} \right)_{L^2(D^k)} &= \left(\sum_{i=1}^d \mathbf{A}_i \frac{\partial \mathbf{v}}{\partial \mathbf{x}_i}, \mathbf{q} \right)_{L^2(D^k)} + \left\langle \frac{1}{2} \mathbf{A}_n \llbracket \mathbf{v} \rrbracket + \frac{\tau_\sigma}{2} \mathbf{A}_n^T \mathbf{A}_n \llbracket \boldsymbol{\sigma} \rrbracket, \mathbf{q} \right\rangle. \end{aligned}$$

We note that, since the right hand side of the WADG formulation is identical to the right hand side of the DG formulation (3), WADG preserves a variant of the energy stability (4).

$$\frac{1}{2} \frac{\partial}{\partial t} \left((T_{1/\rho}^{-1} \mathbf{v}, \mathbf{v})_{\Omega_h} + (T_{\mathbf{C}}^{-1} \boldsymbol{\sigma}, \boldsymbol{\sigma})_{\Omega_h} \right) \leq - \sum_{f \in \Gamma_h} \int_f \frac{\tau_v}{2} |\mathbf{B}_n \llbracket \mathbf{v} \rrbracket|^2 + \frac{\tau_\sigma}{2} |\mathbf{B}_n^T \llbracket \boldsymbol{\sigma} \rrbracket|^2.$$

We note that, for isotropic media, another way to address sub-element variations in material parameters is to diagonalize the matrix \mathbf{C} through a change of variables [31]. This results in uncoupled weighted mass matrices, which can be treated using weight-adjusted approximations for scalar weights. However, this approach is more difficult to apply when \mathbf{C} is anisotropic.

The matrix form of DG

$$\begin{aligned} \mathbf{M}_\rho \mathbf{v}_i &= \mathbf{A}_{v_i} \mathbf{v}_i, & i &= 1, \dots, d \\ \mathbf{M}_\mathbf{C} \boldsymbol{\sigma} &= \mathbf{A}_\sigma \boldsymbol{\sigma}. \end{aligned}$$

where the matrices \mathbf{A}_{v_i} and \mathbf{A}_σ are induced by the discretization of the right hand side.

In d dimensions, the *coupled* mass matrix is given as

$$(\mathbf{M}_{\mathbf{C}^{-1}})_{i_1, \dots, i_{N_d}, j_1, \dots, j_{N_d}} = \int_{D^k} \begin{pmatrix} \phi_{i_1} \\ \vdots \\ \phi_{i_{N_d}} \end{pmatrix}^T \mathbf{C}^{-1} \begin{pmatrix} \phi_{j_1} \\ \vdots \\ \phi_{j_{N_d}} \end{pmatrix}.$$

The storage and inversion of such matrices is expensive,

Weight-adjusted approximation

$$(5) \quad \mathbf{M}_{\mathbf{C}^{-1}} \approx (\mathbf{I} \otimes \mathbf{M}) \mathbf{M}_{\mathbf{C}}^{-1} (\mathbf{I} \otimes \mathbf{M}).$$

We note that, when λ and μ are piecewise constant, the weight-adjusted inner product coincides with exact inversion of the coupled mass matrix. In this case, $\mathbf{M}_{\mathbf{C}}$ reduces to the Kronecker product of the inverse stiffness tensor and the local mass matrix

$$\mathbf{M}_{\mathbf{C}^{-1}} = \mathbf{C}^{-1} \otimes \mathbf{M},$$

which can be explicitly inverted as

$$\mathbf{M}_{\mathbf{C}^{-1}}^{-1} = \mathbf{C} \otimes \mathbf{M}^{-1}.$$

Substituting $\mathbf{M}_{\mathbf{C}^{-1}}^{-1} = \mathbf{C} \otimes \mathbf{M}^{-1}$ into the weight adjusted approximation (5) recovers this expression.

5.1. Energy stability on curvilinear meshes. On affine elements, the skew-symmetric formulation is equivalent to the “strong” DG formulation. This formulation yields an efficient quadrature-free evaluation in terms of derivative and lift matrices, which can be further accelerated by exploiting structure under certain bases [32].

Need to directly discretize skew-symmetric formulation for energy stability on curvilinear meshes.

We note that this formulation is *a-priori* stable, in the sense that a discrete version of energy stability still holds if the L^2 inner products are replaced with discrete inner products computed through inexact quadrature rules. [useful for curvilinear meshes](#).

5.2. Convergence analysis.

6. Numerical experiments.

6.1. Accuracy of weight-adjusted inner products. Show matrix WADG approximation of $T_{\mathbf{W}}^{-1} \mathbf{u}$ is close to $\mathbf{W}^{-1} \mathbf{u}$.

6.2. Verification of stability. Eigenvalue plots with $\tau = 0$ and $\tau = O(1)$ for both square and curvilinear grids with random coefficients close to zero and 1.

6.3. Analytic solutions. We begin by studying the accuracy and convergence of weight-adjusted DG method for several analytical solutions in linear elasticity. In all cases, the solution is expressed in terms of the displacement vector $\mathbf{v}(\mathbf{x}, t)$. Initial conditions for velocity and stress are computed through

$$\mathbf{w}(\mathbf{x}, t) = \frac{\partial \mathbf{v}}{\partial t}, \quad \boldsymbol{\sigma} = \mathbf{C} \mathbf{E} = \mathbf{C} \frac{1}{2} (\nabla \mathbf{v} + \nabla \mathbf{v}^T).$$

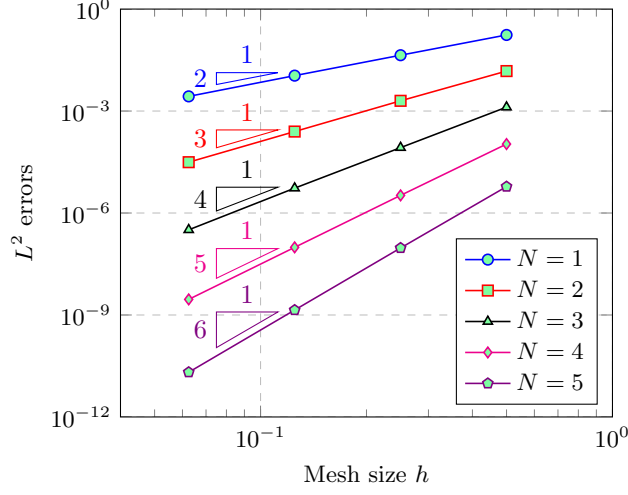


Fig. 1: Convergence of L^2 errors for harmonic oscillation.

Unless otherwise stated, we report relative L^2 errors for all components of the solution

$$\frac{\|\mathbf{v} - \mathbf{v}_h\|_{L^2(\Omega)}}{\|\mathbf{v}\|_{L^2(\Omega)}} = \frac{\left(\sum_{i=1}^m \|\mathbf{v}_i - \mathbf{v}_{i,h}^2\|_{L^2(\Omega)} \right)^{1/2}}{\left(\sum_{i=1}^m \|\mathbf{v}_i\|_{L^2(\Omega)}^2 \right)^{1/2}}.$$

6.3.1. Harmonic oscillation of a square. We first examine convergence on a unit square domain with $\lambda = \mu = \rho = 1$. The displacement is given by

$$\begin{aligned} u_1(x, y, t) &= \cos(\omega\pi t) \cos(\pi x) \sin(\pi y) \\ u_2(x, y, t) &= -\cos(\omega\pi t) \sin(\pi x) \cos(\pi y), \end{aligned}$$

where $\omega = \sqrt{2\mu}$. Figure 1 shows L^2 errors computed at time $T = 1$, using uniform triangular meshes constructed by bisecting a uniform mesh of quadrilaterals along the diagonal. For $N = 1, \dots, 5$, optimal $O(h^{N+1})$ rates of convergence are observed.

6.3.2. Rayleigh and Lamb waves. Next, we examine the convergence of WADG for Rayleigh and Lamb waves, both of which test the imposition of traction-free boundary conditions.

Rayleigh waves are elastic surface waves which decay exponentially away from the surface. These waves are given by the displacement vector

$$\begin{aligned} \mathbf{v}(x, y, t) &= e^{-\omega x \sqrt{1-\xi^2}} \begin{pmatrix} \cos(\omega(y + c_r t)) \\ \sqrt{1-\xi^2} \sin(\omega(y + c_r t)) \end{pmatrix} \\ &+ \left(\frac{\xi^2}{2} - 1 \right) e^{-\omega x \sqrt{1-\frac{\xi^2 \mu}{2\mu+\lambda}}} \begin{pmatrix} \cos(\omega(y + c_r t)) \\ \sin(\omega(y + c_r t)) / \sqrt{1-\frac{\xi^2 \mu}{2\mu+\lambda}} \end{pmatrix}, \end{aligned}$$

where ω is the wavespeed, c_r is the Rayleigh phase velocity $c_r = \xi\sqrt{\mu}$, and ξ satisfies

$$\sqrt{1-\xi^2} \sqrt{1-\frac{\xi^2 \mu}{2\mu+\lambda}} - \left(\frac{\xi^2}{2} - 1 \right)^2 = 0.$$

In our computations, we use $\rho = \mu = \lambda = 1$, $\xi = 0.949554083888034$, and $\omega = 2\pi$. We solve on the domain $[0, 2] \times [0, 1]$ using a sequence of uniform triangular meshes, and enforce traction-free boundary conditions at

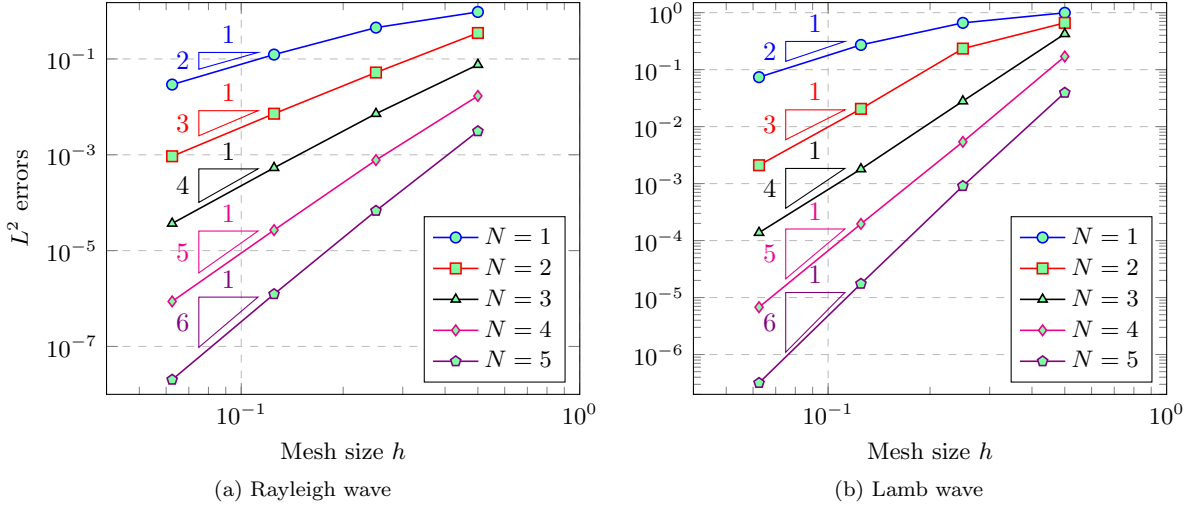


Fig. 2: Convergence of L^2 errors for Rayleigh and Lamb wave solutions.

$x = 0$ and exact Dirichlet boundary conditions at $x = 2$. Periodic boundary conditions are applied at $y = 0$ and $y = 1$.

Lamb waves are supported by elastic waveguides with traction-free (free surface) boundary conditions at the top and bottom of the domain. The displacement of these waves

$$\begin{aligned} v_1(x, y, t) &= (-kB_1 \cos(py) - qB_2 \cos(qy)) \sin(kx - \omega t) \\ v_2(x, y, t) &= (-pB_1 \sin(py) + kB_2 \sin(qy)) \cos(kx - \omega t) \end{aligned}$$

where k is the wavenumber and ω is the frequency, and the constants p and q are defined as

$$p^2 = \frac{\omega^2}{2\mu + \lambda} - k^2, \quad q^2 = \frac{\omega^2}{\mu} - k^2.$$

The wavenumber k and frequency ω are related through a dispersion relation. The ratio of the amplitudes B_1/B_2 can be determined using other parameters, implying that B_1, B_2 are unique up to a scaling constant. In our experiments, we use $\rho = \mu = 1$, $\lambda = 2$, $k = 2\pi$. For these values, $\omega = 13.137063197233$, $B_1 = 126.1992721468$ and $B_2 = 53.88807700007$. We solve on the domain $[-1, 1] \times [-1/2, 1/2]$, with traction-free boundary conditions at $y = \pm 1/2$ and periodic boundary conditions at $x = \pm 1$.

Figure 2b shows L^2 errors for both waves at time $T = 1$. Observed convergence rates fall between the optimal rate of $O(h^{N+1})$ and theoretical rate of $O(h^{N+1/2})$ [33, 34].

6.3.3. Stoneley waves. A Stoneley wave is supported along the interface between two solids [35]. Like Rayleigh waves, Stoneley waves decay exponentially away from the interface, and test the effectiveness of numerical fluxes across interfaces. We follow [4, 36] and use discontinuous media defined by

$$(\rho, \lambda, \mu) = \begin{cases} (10, 3, 3) & y > 0 \\ (1, 1, 1) & y < 0. \end{cases}$$

The displacement vector for a Stoneley wave is then given by

$$\begin{aligned} v_1(x, y, t) &= \begin{cases} \text{Re}((ikB_1e^{-kb_{1p}y} + kb_{1s}B_2e^{-kb_{1s}y})e^{i(ky-\omega t)}), & y > 0 \\ \text{Re}((-kb_{1p}B_1e^{-kb_{1p}y} + ikB_2e^{-kb_{1s}y})e^{i(kx-\omega t)}), & y < 0 \end{cases} \\ v_2(x, y, t) &= \begin{cases} \text{Re}((ikB_3e^{kb_{2p}y} - kb_{2s}B_4e^{kb_{2s}y})e^{i(kx-\omega t)}), & y > 0 \\ \text{Re}((kb_{2p}B_3e^{kb_{2p}y} + ikB_4e^{kb_{2s}y})e^{i(kx-\omega t)}), & y < 0 \end{cases}, \end{aligned}$$

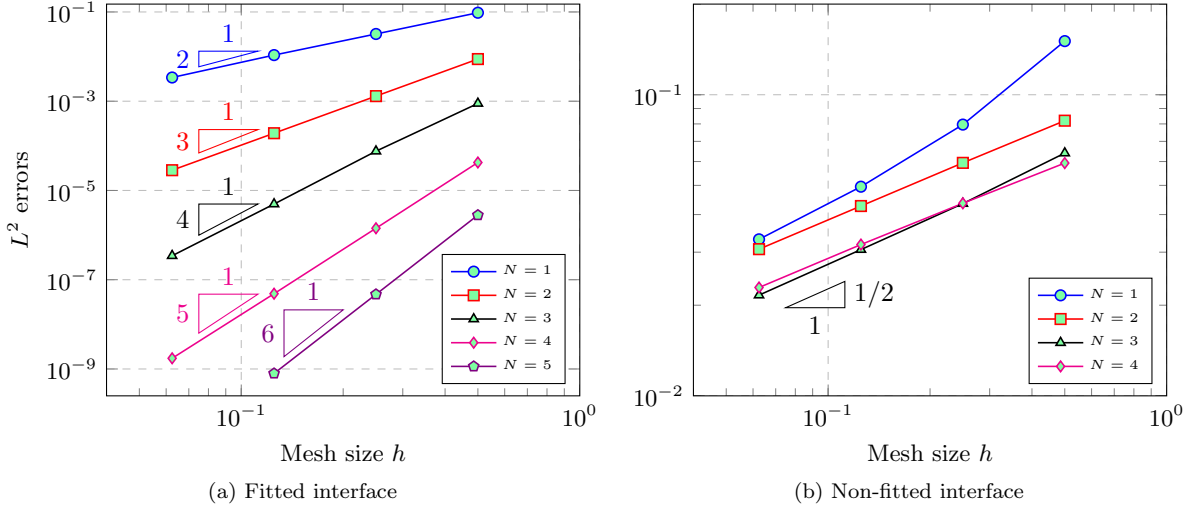


Fig. 3: Convergence of WADG for a Stoneley wave using a fitted mesh aligned with the interface and a non-fitted mesh where the interface does not lie exactly on an element boundary.

where c_{st} is the Stoneley wave speed, and

$$k = \omega/c_{st}, \quad b_{jp} = \sqrt{1 - \frac{c_{st}^2}{(2\mu_j + \lambda_j)/\rho_j}}, \quad b_{js} = \sqrt{1 - \frac{c_{st}^2}{(\mu_j)/\rho_j}}, \quad j = 1, 2.$$

The Stoneley wave speed c_{st} can be determined based material parameters and interface conditions, and the amplitudes B_1, B_2, B_3, B_4 are determined from c_{st} up to scaling by a constant. For the parameters used in this study, we take $c_{st} = 0.546981324213884$, $B_1 = i0.2952173626624$, $B_2 = -0.6798795208473$, $B_3 = i0.5220044931212$, and $B_4 = -0.9339639688697$. We assume $k = 1$, which gives $\omega = c_{st}$.

We solve on the domain $[-1, 1] \times [-5, 5]$, and enforce Dirichlet boundary conditions at all boundaries using the exact solution. Figure 3 shows L^2 errors for two uniform meshes of triangles constructed by bisecting a quadrilateral mesh of $K_{1D} \times 5K_{1D}$ elements. Figure 3a shows errors when K_{1D} is even and the mesh is fitted to the interface at $y = 0$, while Figure 3b shows errors when K_{1D} is odd and the interface cuts through element interiors. When the mesh is fitted to the interface, we observe optimal $O(h^{N+1})$ rates of convergence for $N > 1$.

When the mesh is not fitted to the interface exactly, we compute the application of the weight-adjusted mass matrix inverse using a quadrature rule from Xiao and Gimbutas [37] which is exact for degree $2N + 1$ polynomials. Since the values of ρ, μ , and λ are positive at all quadrature points, the method is energy stable. However, since the exact solution is discontinuous, we expect an $O(1)$ error in elements cut by the interface, resulting in L^2 errors which converge at rate $O(h^{1/2})$. We note that, when using piecewise constant approximations of μ and λ , we observe the same $O(h^{1/2})$ convergence rate, though errors are roughly twice as large in magnitude. [Discuss need to extend WADG to low regularity weights.](#)

6.3.4. Harmonic oscillation of an annulus. This example tests the convergence of WADG for curvilinear mappings.

6.4. Application examples.

6.4.1. Stiff inclusion. Leveque stiff inclusion example.

6.4.2. Heterogeneous anisotropic material. From [7]: discontinuous media with anisotropy on one side, isotropy on the other.

Also do a similar case where random noise is added to both sides and the anisotropy is more strongly discontinuous.

6.5. Three-dimensional example.

Add GPU computations here.

7. Conclusions. Generally applicable to problems with spatially varying matrices $\mathbf{A}_0(\mathbf{x})$, such as in Maxwell’s equations for cloaking problems [38], as well as in vector-valued $H(\text{div})$ or $H(\text{curl})$ functions under matrix-valued mappings such as Piola transforms.

Extension to hybrid meshes is straightforward in 2D [39]. For 3D, care must be taken with pyramids [40, 32].

Formulation allows for the reduction of constant-coefficient RHS costs at high orders using BBDG [41].

8. Acknowledgments. The author gratefully thanks Thomas Hagstrom, Tim Warburton, Axel Modave, and Ruichao Ye for informative discussions.

REFERENCES

- [1] Jesse Chan, Russell J Hewett, and T Warburton. Weight-adjusted discontinuous Galerkin methods: wave propagation in heterogeneous media. *arXiv preprint arXiv:1608.01944*, 2016.
- [2] Jesse Chan, Russell J Hewett, and T Warburton. Weight-adjusted discontinuous Galerkin methods: curvilinear meshes. *arXiv preprint arXiv:1608.03836*, 2016.
- [3] Dimitri Komatitsch, Gordon Erlebacher, Dominik Göddeke, and David Michéa. High-order finite-element seismic wave propagation modeling with MPI on a large GPU cluster. *Journal of computational physics*, 229(20):7692–7714, 2010.
- [4] Lucas C Wilcox, Georg Stadler, Carsten Burstedde, and Omar Ghattas. A high-order discontinuous Galerkin method for wave propagation through coupled elastic–acoustic media. *Journal of Computational Physics*, 229(24):9373–9396, 2010.
- [5] Martin Käser and Michael Dumbser. An arbitrary high-order discontinuous Galerkin method for elastic waves on unstructured meshes - I. The two-dimensional isotropic case with external source terms. *Geophysical Journal International*, 166(2):855–877, 2006.
- [6] Michael Dumbser and Martin Käser. An arbitrary high-order discontinuous Galerkin method for elastic waves on unstructured meshes - II. the three-dimensional isotropic case. *Geophysical Journal International*, 167(1):319–336, 2006.
- [7] Josep de la Puente, Martin Käser, Michael Dumbser, and Heiner Igel. An arbitrary high-order discontinuous Galerkin method for elastic waves on unstructured meshes-IV. Anisotropy. *Geophysical Journal International*, 169(3):1210–1228, 2007.
- [8] Ruichao Ye, Maarten V de Hoop, Christopher L Petrovitch, Laura J Pyrak-Nolte, and Lucas C Wilcox. A discontinuous Galerkin method with a modified penalty flux for the propagation and scattering of acousto-elastic waves. *Geophysical Journal International*, 205(2):1267–1289, 2016.
- [9] Beatrice Riviere and Mary F Wheeler. Discontinuous finite element methods for acoustic and elastic wave problems. *Contemporary Mathematics*, (329):271–282, 2003.
- [10] Béatrice Riviere, Simon Shaw, and JR Whiteman. Discontinuous Galerkin finite element methods for dynamic linear solid viscoelasticity problems. *Numerical Methods for Partial Differential Equations*, 23(5):1149–1166, 2007.
- [11] Sarah Delcourte, Loula Fezoui, and Nathalie Glinsky-Olivier. A high-order discontinuous Galerkin method for the seismic wave propagation. In *ESAIM: Proceedings*, volume 27, pages 70–89. EDP Sciences, 2009.
- [12] Sarah Delcourte and Nathalie Glinsky. Analysis of a high-order space and time discontinuous Galerkin method for elastodynamic equations. Application to 3D wave propagation. *ESAIM: Mathematical Modelling and Numerical Analysis*, 49(4):1085–1126, 2015.
- [13] Jonás D De Basabe, Mrinal K Sen, and Mary F Wheeler. The interior penalty discontinuous Galerkin method for elastic wave propagation: grid dispersion. *Geophysical Journal International*, 175(1):83–93, 2008.
- [14] Paola F Antonietti, Carlo Marcati, Ilario Mazzieri, and Alfio Quarteroni. High order discontinuous galerkin methods on simplicial elements for the elastodynamics equation. *Numerical Algorithms*, 71(1):181–206, 2016.
- [15] Andreas Klöckner, Tim Warburton, Jeff Bridge, and Jan S Hesthaven. Nodal discontinuous Galerkin methods on graphics processors. *Journal of Computational Physics*, 228(21):7863–7882, 2009.
- [16] Nico Gödel, Steffen Schomann, Tim Warburton, and Markus Clemens. GPU accelerated Adams–Bashforth multirate discontinuous Galerkin FEM simulation of high-frequency electromagnetic fields. *Magnetics, IEEE Transactions on*, 46(8):2735–2738, 2010.
- [17] Nico Gödel, Nigel Nunn, Tim Warburton, and Markus Clemens. Scalability of higher-order discontinuous Galerkin FEM computations for solving electromagnetic wave propagation problems on GPU clusters. *Magnetics, IEEE Transactions on*, 46(8):3469–3472, 2010.
- [18] A Modave, A St-Cyr, WA Mulder, and T Warburton. A nodal discontinuous galerkin method for reverse-time migration on gpu clusters. *Geophysical Journal International*, 203(2):1419–1435, 2015.
- [19] Axel Modave, Amik St-Cyr, and Tim Warburton. GPU performance analysis of a nodal discontinuous Galerkin method for acoustic and elastic models. *Computers & Geosciences*, 91:64–76, 2016.
- [20] Cristóbal E Castro, Martin Käser, and Gilbert B Brietzke. Seismic waves in heterogeneous material: subcell resolution of the discontinuous Galerkin method. *Geophysical Journal International*, 182(1):250–264, 2010.
- [21] E Diego Mercier and Nathalie Glinsky. A nodal high-order discontinuous Galerkin method for elastic wave propagation in arbitrary heterogeneous media. *Geophysical Journal International*, 201(2):1101–1118, 2015.

- [22] Mark A Christon. The influence of the mass matrix on the dispersive nature of the semi-discrete, second-order wave equation. *Computer methods in applied mechanics and engineering*, 173(1):147–166, 1999.
- [23] Jean-Luc Guermond and Richard Pasquetti. A correction technique for the dispersive effects of mass lumping for transport problems. *Computer Methods in Applied Mechanics and Engineering*, 253:186–198, 2013.
- [24] Thomas JR Hughes and Jerrold E Marsden. Classical elastodynamics as a linear symmetric hyperbolic system. *Journal of Elasticity*, 8(1):97–110, 1978.
- [25] Jesse Chan and T Warburton. A short note on the penalty flux parameter for first order discontinuous Galerkin formulations. *arXiv preprint arXiv:1611.00102*, 2016.
- [26] Randall J LeVeque. *Finite volume methods for hyperbolic problems*, volume 31. Cambridge university press, 2002.
- [27] Jean-Pierre Berenger. A perfectly matched layer for the absorption of electromagnetic waves. *Journal of computational physics*, 114(2):185–200, 1994.
- [28] Thomas Hagstrom and Timothy Warburton. A new auxiliary variable formulation of high-order local radiation boundary conditions: corner compatibility conditions and extensions to first-order systems. *Wave motion*, 39(4):327–338, 2004.
- [29] Axel Modave, Andreas Atle, Jesse Chan, and Tim Warburton. High-order absorbing boundary conditions with corner/edge compatibility for GPU-accelerated discontinuous Galerkin wave simulations. *arXiv preprint arXiv:1610.05023*, 2016.
- [30] T. Warburton. A low-storage curvilinear discontinuous Galerkin method for wave problems. *SIAM Journal on Scientific Computing*, 35(4):A1987–A2012, 2013.
- [31] V Etienne, E Chaljub, J Virieux, and N Glinsky. An hp-adaptive discontinuous Galerkin finite-element method for 3-D elastic wave modelling. *Geophysical Journal International*, 183(2):941–962, 2010.
- [32] Jesse Chan, Zheng Wang, Axel Modave, Jean-Francois Remacle, and T Warburton. GPU-accelerated discontinuous Galerkin methods on hybrid meshes. *Journal of Computational Physics*, 318:142–168, 2016.
- [33] Claes Johnson and Juhani Pitkäranta. An analysis of the discontinuous Galerkin method for a scalar hyperbolic equation. *Mathematics of computation*, 46(173):1–26, 1986.
- [34] Gerard R Richter. An optimal-order error estimate for the discontinuous Galerkin method. *Mathematics of Computation*, 50(181):75–88, 1988.
- [35] Robert Stoneley. Elastic waves at the surface of separation of two solids. *Proceedings of the Royal Society of London. Series A, Containing Papers of a Mathematical and Physical Character*, 106(738):416–428, 1924.
- [36] An energy-based discontinuous Galerkin discretization of the elastic wave equation in second order form. 2015. Submitted to CMAME.
- [37] H Xiao and Zydrunas Gimbutas. A numerical algorithm for the construction of efficient quadrature rules in two and higher dimensions. *Comput. Math. Appl.*, 59:663–676, 2010.
- [38] Jichun Li and Yunqing Huang. *Time-domain finite element methods for Maxwell’s equations in metamaterials*, volume 43. Springer Science & Business Media, 2012.
- [39] Thomas M Smith, S Scott Collis, Curtis C Ober, James R Overfelt, Hans F Schwaiger, et al. Elastic wave propagation in variable media using a discontinuous Galerkin method. In *2010 SEG Annual Meeting*. Society of Exploration Geophysicists, 2010.
- [40] Jesse Chan and T Warburton. Orthogonal bases for vertex-mapped pyramids. *SIAM Journal on Scientific Computing*, 38(2):A1146–A1170, 2016.
- [41] Jesse Chan and T Warburton. GPU-accelerated Bernstein-Bezier discontinuous Galerkin methods for wave problems. *arXiv preprint arXiv:1512.06025*, 2015.